Optics Letters

Tailoring frequency generation in uniform and concatenated multimode fibers

Z. Sanjabi Eznaveh,[1,*] M. A. Eftekhar,[1] J. E. Antonio Lopez,[1] M. Kolesik,[2] A. Schülzgen,[1] F. W. Wise,[3] D. N. Christodoulides,[1] and R. Amezcua Correa[1]

[1]CREOL, The College of Optics and Photonics, University of Central Florida, Orlando, Florida 32816, USA
[2]College of Optical Sciences, University of Arizona, Tucson, Arizona 85721, USA
[3]School of Applied and Engineering Physics, Cornell University, Ithaca, New York 14853, USA
*Corresponding author: zahoora@knights.ucf.edu

Received 1 December 2016; revised 2 February 2017; accepted 9 February 2017; posted 14 February 2017 (Doc. ID 281710); published 1 March 2017

We demonstrate that frequency generation in multimode parabolic-index fibers can be precisely engineered through appropriate fiber design. This is accomplished by exploiting the onset of a geometric parametric instability that arises from resonant spatiotemporal compression. By launching the output of an amplified Q-switched microchip laser delivering 400 ps pulses at 1064 nm, we observe a series of intense frequency sidebands that strongly depend on the fiber core size. The nonlinear frequency generation is analyzed in three fiber samples with 50 μm, 60 μm, and 80 μm core diameters. We further demonstrate that by cascading fibers of different core sizes, a desired frequency band can be generated from the frequency lines parametrically produced in each section. The observed frequency shifts are in good agreement with analytical predictions and numerical simulations. Our results suggest that core scaling and fiber concatenation can provide a viable avenue in designing optical sources with tailored output frequencies.

OCIS codes: (190.4370) Nonlinear optics, fibers; (190.4410) Nonlinear optics, parametric processes; (190.4380) Nonlinear optics, four-wave mixing; (060.0060) Fiber optics and optical communications.

https://doi.org/10.1364/OL.42.001015

An intense continuous wave (CW) propagating in the anomalous dispersion region of an optical fiber is known to undergo modulation instability (MI). During this process, the CW background breaks up into a train of optical solitons, resulting from the amplification of noise spectral sidebands [1–3]. Modulation instability can also take place in the normal dispersive regime because of cross-phase modulation [4–6], or in systems with periodic variations in either dispersion [7–9] or gain [10,11]. While MI manifests itself purely as a temporal effect in single-mode optical fibers, in multimode fibers this same mechanism is considerably more involved due to the additional spatial degrees of freedom in the transvers plane [12–15].

Quite recently, there has been a growing interest in multimode fibers (MMFs) for next-generation high-capacity telecommunication systems [16–20], and high-energy fiber lasers [21,22]. In light of these investigations, a better understanding of the nonlinear dynamics in MMFs is now imperative. As first shown by Longhi [23], the periodic spatial refocusing of a beam, taking place in a graded-index fiber, can lead to a geometric parametric instability (GPI), regardless of the sign of fiber dispersion. This GPI process has been recently observed in a series of experiments [24,25]. In these studies, this parametric instability was triggered in both the anomalous and normal dispersive regions and produced a series of intense frequency peaks in the visible and near-infrared (NIR) spectral range. Moreover, the presence of many interacting modes introduces multiple pathways for phase-matched nonlinear wave-mixing generation. Consequently, a high-intensity pump pulse propagating in a graded-index MMF can produce an ultrabroadband supercontinuum, beam cleanup, and multimode solitons [24–28]. Multimode fibers offer not only a rich environment to observe a host of new nonlinear interaction phenomena, but also provide a versatile platform for generating a broadband optical supercontinuum with spectral densities that can be orders of magnitude higher (because of much larger cross sections) than those expected from single-mode fiber technologies.

In this Letter, we provide a comprehensive investigation concerning the role of core size scaling on GPI in highly multimode parabolic fibers. The resulting sideband generation was studied in detail in a number of fiber structures with diameters ranging from 50 to 80 μm. In all cases, the sideband frequency shift was found to follow a $a^{-1/2}$ relation, with a being the core radius. In addition, we demonstrate frequency generation in a system of cascaded MMFs having different core sizes. In this case, we find that the output spectrum results from the interplay between the GPI lines induced in each fiber section. These results are in good agreement with analytical predictions and numerical simulations carried out using a generalized unidirectional pulse propagation equation (gUPPE) code [29,30]. This Letter can lead to a new class of light sources with tailored spectral output content.

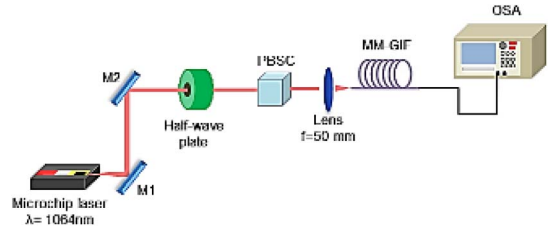

Fig. 1. Schematic representation of the experimental setup. Pulses from a Q-switched microchip laser at 1064 nm are launched into a graded-index MMF. M1 and M2, mirrors; MM-GIF, multimode graded-index fiber; PBSC, polarization beam splitter cube; OSA, optical spectrum analyzer.

Figure 1 shows a schematic representation of the experimental setup. The single-mode output of an amplified Q-switched microchip laser, delivering 95 μJ pulses at 1064 nm, with pulse duration of 400 ps and a repetition rate of 500 Hz, was coupled into the graded-index MMF samples. The free-space coupling efficiency was greater than 85% using a 50 mm focal length lens. A half-wave plate and a polarizing beam splitter cube (PBSC) were used to control the input power. The initial spatial launching conditions were adjusted using a three-axis translation stage. A large set of transverse spatial modes (over 200 modes at 1064 nm) was excited by focusing the laser beam on the front facet of the fiber. Light at the output of the graded-index MMF under test was collected by a multimode patch cord (105 μm core diameter) and analyzed using an optical spectrum analyzer (OSA) with 1 nm resolution, covering the spectral range from 350 to 1750 nm (857.1–171.4 THz). The parabolic multimode fibers used in our experiments were in-house fabricated with core diameters of 50 μm, 60 μm, and 80 μm, and had a maximum refractive index contrast of $\sim 16 \times 10^{-3}$ with respect to the cladding.

Figures 2(a)–2(c) depict a series of rather intense discrete peaks in the visible regime obtained using an optical grating. The pump peak power used was ~185 kW, and the fiber length was ~5 m in all the experiments. As we will see, the main nonlinear mechanisms contributing to the observed sidebands arise from multipath four-wave mixing (FWM) processes and periodic spatiotemporal breathing dynamics. The optical microscope images of the fiber cross sections and their corresponding parabolic refractive index profiles, as measured using a profilometer, are shown in Figs. 2(d)–2(f).

Following the theoretical model of [23], one can show that the spatiotemporal wave instabilities in nonlinear graded-index MMFs can be effectively analyzed in terms of a Floquet–Bloch theory. The periodic expansion/contraction of the beam taking place in graded-index multimode fibers incites modulation instability, regardless of the sign of dispersion [23]. As a result of this mechanism, the periodic spatial breathing of light leads to energy coupling from the pump to the sidebands having frequencies, $\omega_{\mathrm{SB}_m} = \omega_p \pm \sqrt{m}\,\omega_G$ where $\omega_G^2 = 2\delta/|k_0''|$, and δ stands for the regular spacing between the propagation constants of the consecutive modes $\delta = a^{-1}\sqrt{2\Delta}$. Here, $\Delta = (n_{\mathrm{core}} - n_{\mathrm{clad}})/n_{\mathrm{core}}$, and a is the core radius. In the above expression, m is an integer (corresponding to the order of the sidebands), and k_0'' is the fiber dispersion coefficient. At 1064 nm, where the experiments were performed, $k_0'' = 1.6427 \times 10^{-26}$ m^{-1} s^2. In all cases, the input spot size

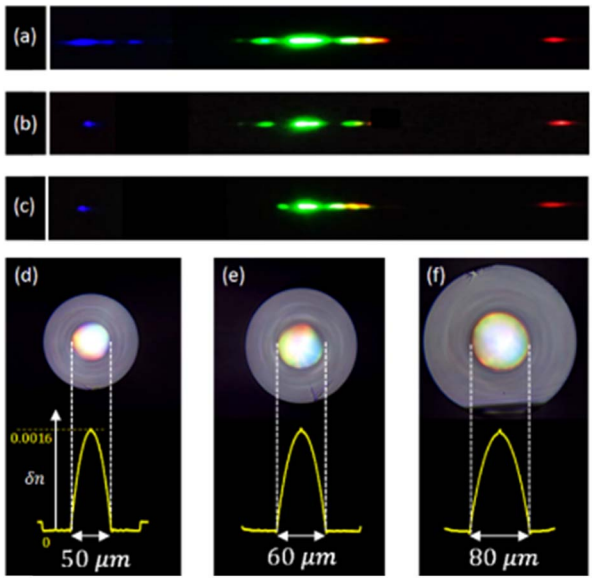

Fig. 2. Images of dispersed visible spectra obtained in a 5 m long graded-index MMF with a (a) 50 μm, (b) 60 μm, and (c) 80 μm core diameter. The peak pump power is 185 kW at 1064 nm. Microscope images of the fabricated fiber samples (d) 50 μm, (e) 60 μm, and 80 μm, along with their corresponding index profiles.

of the laser beam was intentionally chosen to be different than that of the Gaussian fundamental mode LP_{01}, so as to simultaneously excite a large set of LP_{0m} modes, necessary to initiate the required periodic spatial compression. Based on the aforementioned fiber parameters, the spatiotemporal oscillation periods $z_0 = \pi a/\sqrt{2\Delta}$ are approximately 550 μm, 661 μm and 881 μm for the three core diameters of 50 μm, 60 μm, and 80 μm, respectively. Accordingly, from these values, the first sidebands ($m = 1$ in the visible) are expected to be observed at 414.61, 403.05, and 386.83 THz. Table 1 provides the location of the first five sidebands $m = 1, 2, \ldots$, predicted by the theory based on the presented parameters. Similarly, the other discrete peaks in the visible (shown in Fig. 2) result from higher-order lines ω_m and their respective FWM combinations.

To better understand the experimental observations, numerical simulations were carried out based on a gUPPE approach. In doing so, the spatiotemporal evolution of the total electric field in the presence linear and nonlinear effects is computed at each step. Unlike conventional beam propagation schemes that typically handle a finite number of modes, the gUPPE approach allows one to simultaneously follow the evolution of hundreds or thousands of modes (as in out experiments) [29,30]. The field contribution to each spatial mode can then be determined by projection. Using this approach, an arbitrary number of modes can be simultaneously analyzed. Linear (dispersion, guiding) and nonlinear effects (self-phase modulation (SPM), FWM, third harmonic generation, shock, and Raman effects) are accounted for in our code. In our simulations, the time window was 6 ps, the size of the spatial window was 70 μm×70 μm, and an adaptive integration step size of 1–2 μm was used. The spatial and temporal grid used was 64 × 64 and 8192, respectively. The pulse width was taken to be 400 fs, and a beam waist of 27 μm was assumed at the fiber input. We note that our simulations are not particularly

Table 1. First Five Visible Sidebands Predicted by [23] for the Three Fiber Samples

Core Diameter	First Sideband [THz]	Second Sideband [THz]	Third Sideband [THz]	Fourth Sideband [THz]	Fifth Sideband [THz]
50 μm	414.61	469.55	511.72	547.26	578.57
60 μm	403.05	453.21	491.70	524.14	552.73
80 μm	386.83	430.26	463.60	491.70	516.45

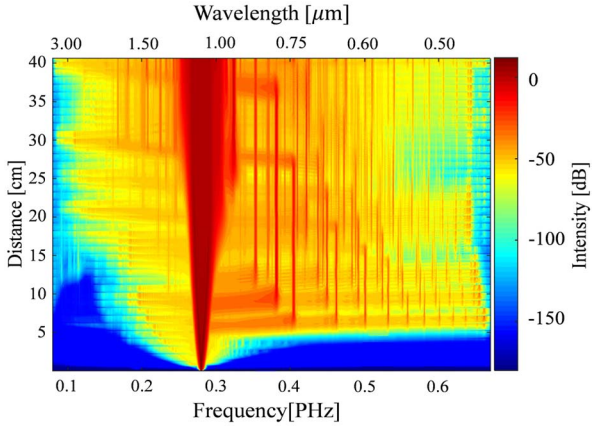

Fig. 3. Spectral evolution upon propagation in a ∼40 cm graded-index MMF with a 50 μm core diameter, as obtained from gUPPE simulations. Several lines emerge in the visible after a distance of ∼7 cm.

sensitive to the duration of the input pulse. In all our calculations, the propagation distance was 40 cm. As an example, Fig. 3 illustrates the spectral evolution as a function of the propagation distance in the graded-index MMF with a 50 μm core diameter.

In this figure, the spectral broadening due to SPM can be clearly seen during the early stages of propagation. Subsequently, after ∼7 cm, a series of sidebands emerge (extending from NIR to the visible) with the first one located at 724 nm. On the other hand, after 20 cm of propagation, the first GPI induced NIR line at ∼2 μm appears. More spectral features eventually emerge as a result of Raman and FWM intermixing. Our simulations indicate that the first sideband is always the most intense compared to the rest. In a similar fashion, the two other fiber samples were simulated.

Figure 4 compares the frequency positions of the induced GPI sidebands observed experimentally with those expected from numerical and analytical results for the three fibers under consideration. The spectra were measured using an OSA covering the wavelength range between 350 and 1750 nm. The generated spectra were stable over several hours. In this figure, the dashed green lines represent the frequency positions, as expected from analytical results. Meanwhile, the black and blue solid curves illustrate the simulated and measured spectra, respectively. This figure indicates that there is an excellent agreement between the experimental observations, numerical simulations, and theoretical predictions. In Figs. 4(a) and 4(c), corresponding to core diameters of 50 μm and 80 μm, the numerical and experimental results agree well up to the fifth sideband. In Fig. 4(b), the second sideband was not particularly visible. Both theory and simulations predict that for every anti-Stokes GPI sideband, there should be a corresponding

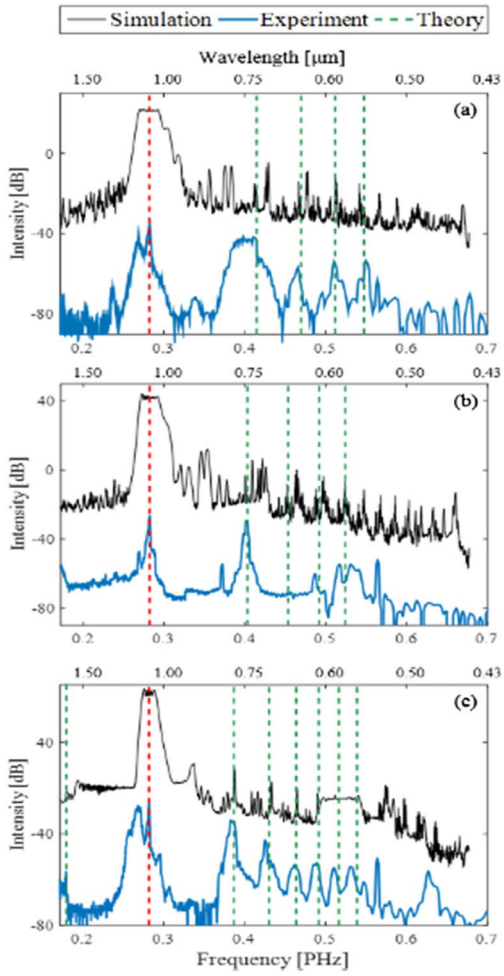

Fig. 4. Simulated (black curve) and measured (blue curve) spectra unfolding in a parabolic multimode fiber with a (a) 50 μm,(b) 60 μm, and (c) 80 μm core diameter. The red dotted lines represent the position of the pump at 1064 nm, while the green lines indicate the position of the expected GPI induced sidebands. A redshift in the sidebands proportional to $a^{-1/2}$ is observed as the core diameter increases.

Stokes counterpart with an equal frequency detuning from the pump. However, due to the limited operational range of our OSA, we were unable to observe the NIR Stokes spectral peaks for our fibers with 50 and 60 μm core diameters. However, the first Stokes line for an 80 μm core fiber was observed at ∼1684 nm. Our theoretical analysis indicates that a change in the core diameter from 50 μm to 80 μm, can redshift the position of the first sideband ($m = 1$) by $\Delta f = 28$ THz (∼100 nm). For higher order sidebands ($m > 1$), this shift scales according to $\sqrt{m}\,\Delta f$. Here, it is worth mentioning that increasing Δ results in the opposite effect as compared to enlarging the core, i.e., it leads to a blueshift in the position

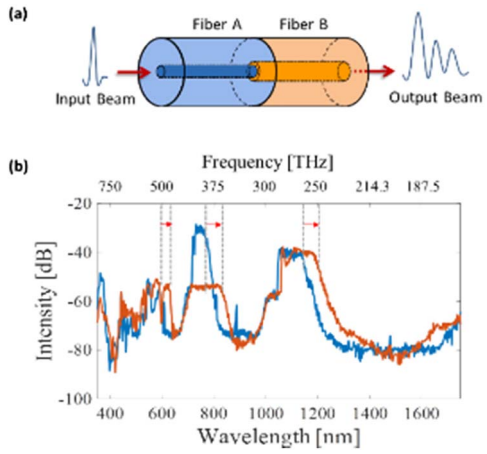

Fig. 5. (a) Schematic of a cascaded system consisting of two MMFs with different core diameters. (b) Measured spectra at the output of a 5 m long fiber with 50 μm core diameter (blue) and for a cascaded system composed of two 2.5 m long fiber segments with 50 and 80 μm core diameters (orange).

of the frequency sidebands. These unique nonlinear effects in parabolic index fibers can be potentially exploited in designing novel light sources with a tailored spectral content.

Finally, we experimentally consider nonlinear frequency generation in a system involving two different parabolic MMFs in cascade, as shown in Fig. 5(a). The core diameters of these segments were 50 and 80 μm, respectively. Each section was 2.5 m long. Figure 5(b) compares the frequency spectrum generated in a 5 m long parabolic-index MMF with a 50 μm core diameter (blue) with that in the aforementioned cascaded system (orange). In all cases, the fiber is excited at the center with the peak power of 185 kW at 1064 nm. This figure clearly shows the observed spectral lines in the concatenated fibers have experienced broadening. This can be understood given that the GPI-induced sidebands of the 80 μm core diameter fiber are redshifted with respect to those produced in the 50 μm core fiber (Fig. 4). Concatenation of these two fibers leads to a nonlinear interaction between these two sets of frequency sidebands, which manifests itself as a broadening of the spectrum toward longer wavelengths. It should be noted that, in all cases, we found the resulting spectrum to be stable, controllable, and repeatable.

In conclusion, we have systematically investigated the impact of fiber core size on the frequency sideband generation induced by geometric parametric instability in a graded-index MMF when pumped in the normal dispersive region. The theoretically expected redshift in GPI lines is experimentally verified in a set of parabolic fibers with increasing diameters. Moreover, we demonstrated that the spectral content can be further engineered by concatenating multimode fibers of appropriate core sizes. The observed frequency generation can be accurately predicted based on analytical models and numerical simulations. Of interest will be to study these processes in tapered multimode optical fibers that could, in turn, be used to optimize supercontinuum generation with very high spectral power densities. In addition, investigating the onset of GPI sidebands in periodically varying graded-index MMFs can also be another interesting direction.

Funding. Office of Naval Research (ONR) (MURI N00014-13-1-0649); HEL-JTO (W911NF-12-1-0450); Army Research Office (ARO) (W911NF-12-1-0450); Air Force Office of Scientific Research (AFOSR) (FA9550-15-10041); National Science Foundation (NSF) (ACI-1053575).

Acknowledgment. This Letter used the Extreme Science and Engineering Discovery Environment (XSEDE).

REFERENCES

1. A. Hasegawa and W. Brinkman, IEEE J. Quantum Electron. **16**, 694 (1980).
2. K. Tai, A. Hasegawa, and A. Tomita, Phys. Rev. Lett. **56**, 135 (1986).
3. S. Trillo and S. Wabnitz, Opt. Lett. **16**, 986 (1991).
4. G. P. Agrawal, Phys. Rev. Lett. **59**, 880 (1987).
5. S. Wabnitz, Phys. Rev. A **38**, 2018 (1988).
6. M. Haelterman and M. Badolo, Opt. Lett. **20**, 2285 (1995).
7. F. Consolandi, C. De Angelis, A.-D. Capobianco, G. Nalesso, and A. Tonello, Opt. Commun. **208**, 309 (2002).
8. M. Droques, A. Kudlinski, G. Bouwmans, G. Martinelli, and A. Mussot, Opt. Lett. **37**, 4832 (2012).
9. C. Finot, J. Fatome, A. Sysoliatin, A. Kosolapov, and S. Wabnitz, Opt. Lett. **38**, 5361 (2013).
10. S. M. J. Kelly, Electron. Lett. **28**, 806 (1992).
11. F. Matera, A. Mecozzi, M. Romagnoli, and M. Settembre, Opt. Lett. **18**, 1499 (1993).
12. J. V. Moloney and A. C. Newell, *Nonlinear Optics* (Westvie, 2004).
13. B. A. Malomed, D. Mihalache, F. Wise, and L. Torner, J. Opt. B **7**, R53 (2005).
14. F. Poletti and P. Horak, J. Opt. Soc. Am. B **25**, 1645 (2008).
15. A. Mafi, J. Lightwave Technol. **30**, 2803 (2012).
16. R. Ryf, N. K. Fontaine, M. A. Mestre, S. Randel, X. Palou, C. Bolle, A. H. Gnauck, S. Chandrasekhar, X. Liu, B. Guan, R.-J. Essiambre, P. J. Winzer, S. Leon-Saval, J. Bland-Hawthorn, R. Delbue, P. Pupalaikis, A. Sureka, Y. Sun, L. Grüner-Nielsen, R. V. Jensen, and R. Lingle, *12 × 12 MIMO Transmission Over 130-km Few-Mode Fiber* (Optical Society of America, 2012), paper FW6C.4.
17. D. J. Richardson, J. M. Fini, and L. E. Nelson, Nat. Photonics **7**, 354 (2013).
18. R. G. H. van Uden, R. A. Correa, E. A. Lopez, F. M. Huijskens, C. Xia, G. Li, A. Schülzgen, H. de Waardt, A. M. J. Koonen, and C. M. Okonkwo, Nat. Photonics **8**, 865 (2014).
19. A. M. Velazquez-Benitez, J. C. Alvarado, G. Lopez-Galmiche, J. E. Antonio-Lopez, J. Hernández-Cordero, J. Sanchez-Mondragon, P. Sillard, C. M. Okonkwo, and R. Amezcua-Correa, Opt. Lett. **40**, 1663 (2015).
20. P. Sillard, D. Molin, M. Bigot-Astruc, K. D. Jongh, F. Achten, A. M. Velázquez-Benítez, R. Amezcua-Correa, and C. M. Okonkwo, J. Lightwave Technol. **34**, 425 (2016).
21. X. Zhu, A. Schülzgen, H. Li, L. Li, Q. Wang, S. Suzuki, V. L. Temyanko, J. V. Moloney, and N. Peyghambarian, Opt. Lett. **33**, 908 (2008).
22. D. J. Richardson, J. Nilsson, and W. A. Clarkson, J. Opt. Soc. Am. B **27**, B63 (2010).
23. S. Longhi, Opt. Lett. **28**, 2363 (2003).
24. K. Krupa, A. Tonello, A. Barthélémy, V. Couderc, B. M. Shalaby, A. Bendahmane, G. Millot, and S. Wabnitz, Phys. Rev. Lett. **116**, 183901 (2016).
25. G. Lopez-Galmiche, Z. Sanjabi Eznaveh, M. A. Eftekhar, J. Antonio Lopez, L. G. Wright, F. Wise, D. Christodoulides, and R. Amezcua Correa, Opt. Lett. **41**, 2553 (2016).
26. L. G. Wright, W. H. Renninger, D. N. Christodoulides, and F. W. Wise, Opt. Express **23**, 3492 (2015).
27. L. G. Wright, D. N. Christodoulides, and F. W. Wise, Nat. Photonics **9**, 306 (2015).
28. K. Krupa, A. Tonello, B. M. Shalaby, M. Fabert, A. Barthélémy, G. Millot, S. Wabnitz, and V. Couderc, arXiv:160302972 (2016).
29. M. Kolesik and J. V. Moloney, Phys. Rev. E **70**, 36604 (2004).
30. J. Andreasen and M. Kolesik, Phys. Rev. E **86**, 36706 (2012).